ACS chemical biology

Articles

pubs.acs.org/acschemicalbiology

Iron–Sulfur Cluster Engineering Provides Insight into the Evolution of Substrate Specificity among Sulfonucleotide Reductases

Devayani P. Bhave,[†] Jiyoung A. Hong,[‡] Rebecca L. Keller,[¶] Carsten Krebs,[¶,≠] and Kate S. Carroll[†,‡,§,*]

[†]Chemical Biology Graduate Program and [‡]Department of Chemistry, University of Michigan, Ann Arbor, Michigan 48109, United States

Departments of [¶]Biochemistry and Molecular Biology and [≠]Chemistry, The Pennsylvania State University, University Park, Pennsylvania 16802, United States

[§]Department of Chemistry, The Scripps Research Institute, Jupiter, Florida 33458, United States

Supporting Information

ABSTRACT: Assimilatory sulfate reduction supplies prototrophic organisms with reduced sulfur that is required for the biosynthesis of all sulfur-containing metabolites, including cysteine and methionine. The reduction of sulfate requires its activation *via* an ATP-dependent activation to form adenosine-5′-phosphosulfate (APS). Depending on the species, APS can be reduced directly to sulfite by APS reductase (APR) or undergo a second phosphorylation to yield 3′-phosphoadenosine-5′-phosphosulfate (PAPS), the substrate for PAPS reductase (PAPR). These essential enzymes have no human homologue, rendering them attractive targets for the development of novel antibacterial drugs. APR and PAPR share sequence and structure homology as well as a common catalytic mechanism, but the enzymes are distinguished by two features, namely, the amino acid sequence of the phosphate-binding loop (P-loop) and an iron–sulfur cofactor in APRs. On the basis of the crystal structures of APR and PAPR, two P-loop residues are proposed to determine substrate specificity; however, this hypothesis has not been tested. In contrast to this prevailing view, we report here that the P-loop motif has a modest effect on substrate discrimination. Instead, by means of metalloprotein engineering, spectroscopic, and kinetic analyses, we demonstrate that the iron–sulfur cluster cofactor enhances APS reduction by nearly 1000-fold, thereby playing a pivotal role in substrate specificity and catalysis. These findings offer new insights into the evolution of this enzyme family and extend the known functions of protein-bound iron–sulfur clusters.

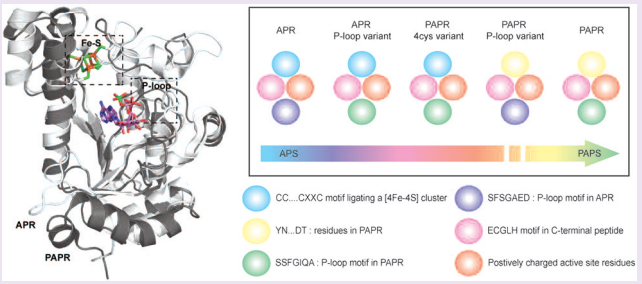

Assimilatory sulfate reduction supplies prototrophic organisms with reduced sulfur that is required for the biosynthesis of all sulfur-containing metabolites, including the amino acids cysteine and methionine.[1,2] The reduction of sulfate requires its activation by an ATP-dependent activation to form adenosine-5′-phosphosulfate (APS). For incorporation of sulfur into biomolecules, the sulfate in APS must be reduced to sulfite and finally into sulfide. In plants, algae, and many bacteria, APS can be reduced directly to sulfite by APS reductase (APR); alternatively, in fungi, some cyanobacteria, and γ-proteobacteria, this compound requires a second phosphorylation step to yield 3′-phosphoadenosine-5′-phosphosulfate (PAPS), the substrate for PAPS reductase (PAPR; Scheme 1, Table 1, and Figure 1). These essential enzymes, collectively known as sulfonucleotide reductases (SRs), have no human homologue, rendering them an attractive target for the development of novel antibacterial drugs and herbicides.[3−6]

The importance of SRs for microbial and plant survival has motivated investigations of their catalytic mechanism and structure.[6−14] These studies support the mechanism shown in Scheme 2, which involves nucleophilic attack by a conserved C-terminal cysteine residue on the substrate leading to the formation of a covalent enzyme *S*-sulfocysteine intermediate. Sulfite is then released by thiol-disulfide exchange with free thioredoxin (Trx) in bacterial and fungal SRs or through the action of a C-terminal Trx-like domain in plants. Therefore, the general features of the thiol reaction chemistry are shared despite the differences in substrate. SRs are homologous in sequence (~25% identity; Supplementary Figure 1), particularly

Scheme 1. Reaction Catalyzed by Sulfonucleotide Reductases

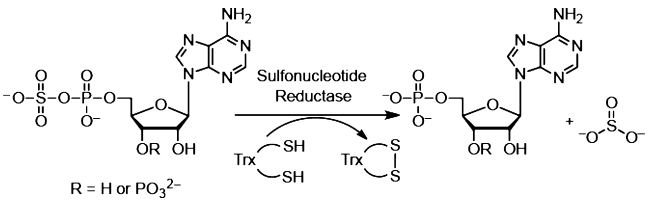

Received: July 24, 2011
Accepted: October 24, 2011
Published: October 24, 2011

Table 1. Apparent Second-Order Rate Constants (k_{cat}/K_m) for Assimilatory SRs[a]

	iron–sulfur cluster	substrate	k_{cat}/K_m (M^{-1} min^{-1})	preference[b]
P. aeruginosa APR[c]	yes	APS	2.0×10^8	APS
		PAPS	1.6×10^4	
M. tuberculosis APR[c]	yes	APS	2.5×10^8	APS
		PAPS	6.0×10^4	
B. subtilis APR[d]	yes	APS	3.1×10^6	none
		PAPS	1.6×10^6	
A. thaliana APR2[e]	yes	APS	3.8×10^8	APS
		PAPS[e]	1.3×10^4	
P. patens APR[e]	yes	APS	3.8×10^8	APS
		PAPS[e]	3.8×10^4	
E. coli PAPR[c]	no	APS	7.2×10^2	PAPS
		PAPS	2.3×10^8	
P. patens APR-B[e]	no	APS	2.1×10^5	APS
		PAPS	2.2×10^2	

[a]Activities were measured with purified recombinant enzymes, as production of sulfite from varying concentrations of [^{35}S]-APS and [^{35}S]-PAPS, in the presence of DTT and recombinant thioredoxin from *E. coli* as the electron donor. [b]Defined as difference in substrate utilization of $\geq 10^2$. [c]Measured at pH 8.0. [d]Measured at pH 8.0.[18] [e]Measured at pH 9.0.[19] [f]Value estimated as the upper limit from ref 19.

within active site residues that line the active site (~50% identity and 75% similarity; Supplementary Figure 2) and share a common three-dimensional structure (1.2 Å rms deviation; Figure 2, panel a).[8,15] The SR monomer adopts a Rossman-like fold and is characterized by four conserved structural elements that define the active site: the LTDG motif, phosphate-binding loop (P-loop), Arg-loop, and C-terminal ECGLH segment with the catalytic cysteine (Supplementary Figure 1).

Upon closer inspection, sequence and structure alignments reveal two key differences between APR and PAPR, namely, the amino acid sequence of the P-loop and the presence of the cysteine motif, CC...CXXC, in APR. The P-loop of APR is typically composed of an SFS–GAED motif, while the corresponding sequence in PAPR is SSSFGIQA (Figure 1, panels a and b). In contrast to the typical role for the P-loop in binding a 5′-phosphate group, crystal structures show that the P-loop interacts with the APS O3′ hydroxyl or the PAPS 3′-phosphate (Figure 2, panels b and c). The four additional cysteine residues in APR coordinate an iron–sulfur cluster, whereas the cofactor is replaced by the YN...DXXT motif in PAPR (Figure 1, panels a and c; Figure 2, panels d and e). Functional analysis indicates that when the [4Fe-4S] cofactor is present, it is required for catalytic activity; however, the cluster is not involved in redox chemistry and does not bind directly to APS.[6,8,16,17] Two interesting exceptions exist in *Bacillus subtilis*, which harbors the cluster but can utilize both APS and PAPS as substrates [Bs(P)APR],[18] and the moss *Physcomitrella patens*, which lacks the cysteine pairs and associated cofactor yet can reduce APS (PpAPR-B).[19] Notably, these SR variants exhibit 100- to 1000-fold decreases in their second-order rate constants (k_{cat}/K_m) for substrate reduction (Table 1). On the basis of the aforementioned observations, it has been proposed that the P-loop is the principle determinant of substrate specificity in these enzymes[7–10] and that the [4Fe-4S] cluster plays a structural and/or regulatory role.[8,16,18]

Much effort has been made to understand substrate specificity in enzymes, and several attempts have been made to rationally alter the specificity of an enzyme with sequence

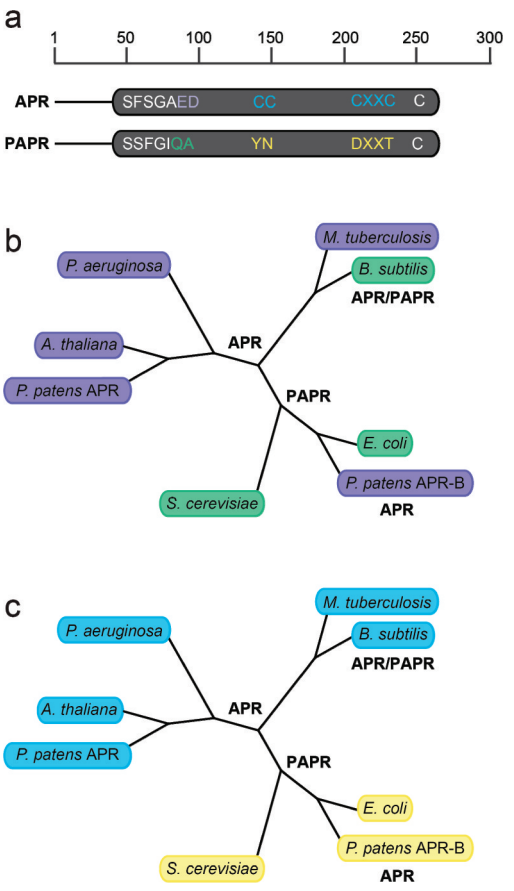

Figure 1. Domain organization and phylogenetic classification in the sulfonucleotide reductase family. (a) Bacterial APRs possess the cysteine motif CC...CXXC that coordinates a [4Fe-4S] cluster (blue). In PAPRs, conserved residues replace the cysteine motif (yellow). The P-loop in APR is terminated by two negatively charged residues (purple). The 3′-phosphate moiety of PAPS can be accommodated by the P-loop motif of PAPR as it bears residues with small and neutral side chains (green). (b, c) Dendrograms illustrating the sequence homology between enzymes within the SR family. The sequence alignment was performed using ClustalW, and the tree was constructed using the Geneious program. Each subclass of SR is clearly delineated: APRs from higher plants with their unique C-terminal domain (*A. thaliana*, *P. patens*-APR), bacterial APRs (*P. aeruginosa*, *M. tuberculosis*, *B. subtilis*), and PAPRs (*E. coli*, *P. patens*-APR-B, and *S. cerevisiae*). Differentiation in the (b) P-loop region and (c) iron–sulfur cluster coordinating residues of the SRs is indicated by color: purple, APR-like; green, PAPR-like; blue, possessing the [4Fe-4S] cluster; yellow, lacking the [4Fe-4S] cluster. APR from *B. subtilis* is unique and can reduce both APS and PAPS.

Scheme 2. Proposed Mechanism of Sulfonucleotide Reduction

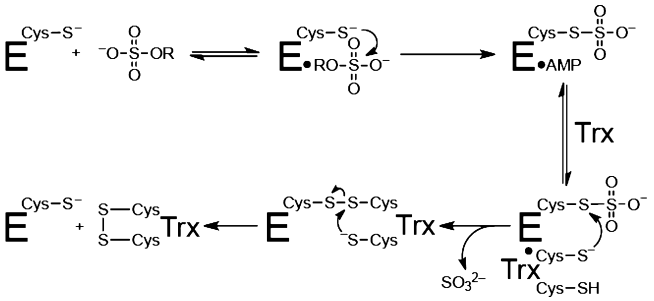

dx.doi.org/10.1021/cb200261n | ACS Chem. Biol. 2012, 7, 306–315

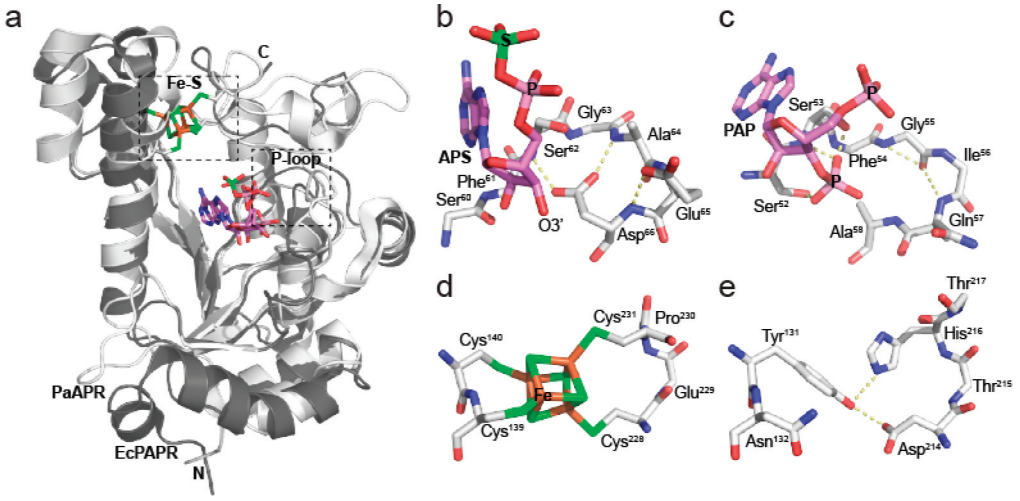

Figure 2. Comparison of putative substrate binding elements in SRs. (a) Superposition of the structures of EcPAPR in charcoal (PDB 2O8V) and PaAPR in white (PDB 2GOY) showing the positions of the [4Fe-4S] cluster, P-loop region, and APS or PAP ligand (modeled from PDB 2OQ2). Comparison between the P-loop regions of (b) PaAPR bound to APS and (c) EcPAPR bound to PAP. Hydrogen bonding interactions are indicated by yellow dashes. Comparison of (d) the iron–sulfur cluster coordination site in PaAPR and (e) the corresponding semiconserved residues in EcPAPR.

and structural information as the blueprint for redesign.[20] One of the first successful examples was of changing the coenzyme specificity of *Escherichia coli* glutathione reductase from NADP to NAD.[21] Structurally, NADP and NAD differ by a phosphate group at the 3′-postition of the adenosine 5′-phosphate (AMP) moiety, reminiscent of APS and PAPS. In glutathione reductase, the switch in coenzyme preference was accomplished by changing amino acids within the P-loop. Similarly, protein engineering has been used successfully by Shokat and coworkers to alter the nucleotide specificity of the prototypical tyrosine kinase, Src, to accept non-native nucleotides.[22] This concept was subsequently extended to redesign kinase active sites to accept unique nucleotide inhibitors to facilitate direct identification of kinase targets.[23] Overall these studies demonstrate that enzyme redesign is a powerful tool in exploiting substrate recognition elements to elucidate the catalytic mechanism and function of an enzyme.

Although it has been proposed that SR substrate specificity is dictated by the P-loop, this hypothesis has not yet been tested and, moreover, does not address the potential role of the iron–sulfur cluster. To gain insight into the forces driving specificity and catalytic efficiency of SRs we have employed metalloprotein engineering, spectroscopic, and kinetic analyses. On the basis of our findings, we propose that the iron–sulfur cluster is a major determinant of specificity in this family of enzymes, specifically by enhancing the efficacy of the chemical step of catalysis. In this way, our findings offer new perspectives on the evolution of SRs and the function of protein-bound iron–sulfur clusters and hold value for the development of inhibitors for SRs, a validated target for antibacterial therapy, including tuberculosis.[5,24,25]

RESULTS AND DISCUSSION

The P-loop residues in APRs have the SFS–GAED motif, while the corresponding motif in PAPR consists of SSSFGIQA. In APR, the glutamate and aspartate residues interact with three P-loop amide groups and are positioned above the dipole of the α3 helix, as if they were mimicking the interaction of a negatively charged phosphate (Figure 2, panels b and c). Conversely, the replacement of these acidic residues with Gln and Ala in PAPR would facilitate interaction of the amide groups with a 3′-phosphate and accommodate the bulkier moiety. To investigate this proposal, we generated E65Q, D66A, and E65Q D66A variants of APR from *Pseudomonas aeruginosa* (PaAPR) as well as Q57E, A58D, and Q57E A58D variants of PAPR from *Escherichia coli* (EcPAPR). Of note, the enzymes from these particular species were chosen on the basis of available structural and functional information. We first tested the activity of the variants with native and non-native substrates. Interestingly, none of these substitutions increased k_{cat}/K_m for the non-native substrate (Supplementary Table 1). In addition, the D66A and E65Q single substitutions in PaAPR had at most a 10-fold effect on APS reduction, whereas the Q65E and A58D replacements in EcPAPR exhibited a 1000-fold effect on the reduction of PAPS. All double variants were significantly impaired relative to their wild-type counterparts. To complement this analysis, we measured the dissociation constants (K_d) for the reaction products AMP and 3′-phosphoadenosine-5′-phosphate (PAP) for the P-loop variants (Figure 3). PaAPR variants showed at most a 2.5-fold enhancement in PAP binding, whereas no EcPAPR substitution enhanced association with AMP. Analogous to kinetic studies, the binding of P-loop variants to the native ligand was diminished, relative to the wild-type enzyme. Overall, this analysis shows that modification of the P-loop decreases binding and catalysis for the native ligand; however, the converse does not hold true as amino acid replacements do not correlate with enhancements for the non-cognate substrate or ligand.

As the P-loop substitutions did not succeed in altering substrate specificity, a possible contribution for the iron–sulfur cluster was investigated. On the basis of the similar three-dimensional fold of APR and PAPR, we reasoned that EcPAPR residues (Y131, N132, D214, and T217) might be replaced by cysteine and enable coordination of an iron–sulfur cluster (Figure 2, panels d and e). Thus, site-directed mutagenesis was employed, and the resulting protein was coexpressed in bacteria with the pDB1282 plasmid that harbors the *isc* operon for cluster assembly.[26] This approach afforded 10 mg of protein per liter of culture. The resulting enzyme, termed EcPAPR4cys, eluted as a dimer from the gel filtration column, analogous to

dx.doi.org/10.1021/cb200261n | *ACS Chem. Biol.* 2012, 7, 306–315

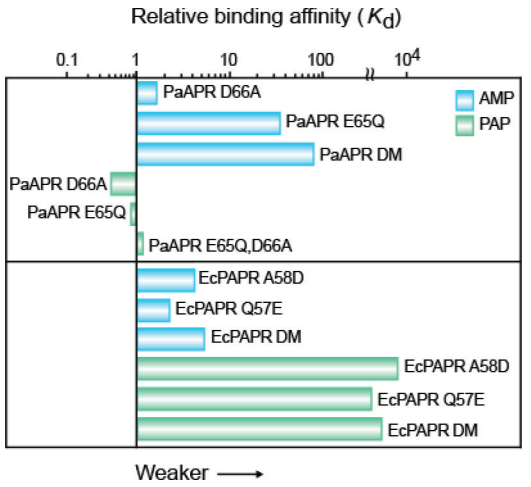

Figure 3. Relative change in ligand dissociation constants for wild-type APR or PAPR and P-loop variants. The ratio of K_d values is plotted relative to wild-type enzymes. Blue and green bars indicate inhibition by AMP and PAP, respectively. DM indicates E65Q D66A PaAPR or Q57E A58D EcPAPR. K_d values and other kinetic parameters for all proteins are presented in Supplementary Table 1.

wild-type EcPAPR, and the purity was estimated to be greater than 95% (Figure 4, panel a). The UV–vis absorbance spectrum of EcPAPR4cys showed a maximum in the visible range at 410 nm, which is similar to the [4Fe-4S] chromophore of PaAPR (Figure 4, panel a).[16] However, ICP analysis of EcPAPR4cys showed that each mole of protein contained only 2.3 mol of iron. The amount of iron could not be increased by reconstitution or anaerobic purification (data not shown).

To identify the types and relative incorporation of iron–sulfur clusters in EcPAPR4cys, we employed a combination of Mössbauer and EPR spectroscopies and analytical methods. ICP analysis of a sample of EcPAPR4cys enriched in ^{57}Fe for Mössbauer spectroscopy reveals 2.0 Fe per polypeptide. The 4.2-K/53-mT Mössbauer spectrum of this sample (Figure 4, panel b) shows that the majority (82%) of the iron associated with EcPAPR gives rise to a quadrupole doublet with parameters typical of $[4Fe\text{-}4S]^{2+}$ clusters: isomer shift (δ) of 0.45 mm/s and quadrupole splitting parameter (ΔE_Q) of 1.03 mm/s. The remaining iron (15%) exhibited properties reminiscent of a $[2Fe\text{-}2S]^{2+}$ cluster (δ = 0.27 mm/s, ΔE_Q = 0.57 mm/s). The $[2Fe\text{-}2S]^{2+}$ form is also observed in plant and bacterial APRs and most likely results from partial degradation of the [4Fe-4S] cluster.[16,18] An identical EPR sample does not reveal the spectroscopic signatures of paramagnetic Fe/S clusters with S = 1/2 ground state (data not shown). Taken together, Mössbauer and ICP analyses indicate that approximately half of all EcPAPR4cys monomers coordinate a [4Fe-4S] cluster.

Although the iron–sulfur cluster in APR does not undergo redox chemistry during catalysis, the reduced form of the cluster can serve as a useful tool for characterization and mechanistic studies. Along these lines, we have recently characterized the 1+ state of the [4Fe-4S] cluster in APR from *Mycobacterium tuberculosis* (MtAPR) using electron paramagnetic resonance (EPR) spectroscopy.[16] Optimal reduction of the iron–sulfur cluster in EcPAPR4cys was achieved using the photoactivatable catalyst 5-deazaflavin in the presence of sodium oxalate. Like MtAPR, the EPR signal of the reduced EcPAPR4cys is broad but shows rhombic symmetry with apparent g-values of 2.07, 1.90, and 1.76, which are characteristic of a [4Fe-4S] cluster in the 1+ state (Figure 4, panel c). Spin quantitation of the EPR

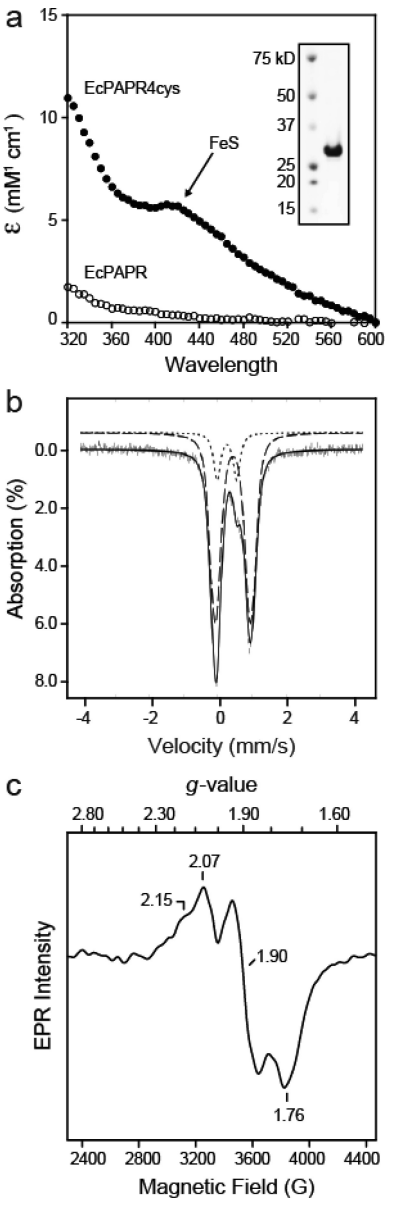

Figure 4. Spectroscopic characterization of EcPAPR4cys. (a) UV–vis absorption spectra of EcPAPR and EcPAPR4cys. UV–vis absorption of 10 μM EcPAPR (○) or EcPAPR4cys (●) in buffer containing 50 mM Tris–HCl, 150 mM NaCl (pH 7.4 at 25 °C), and 10% (v/v) glycerol. Inset: Coomassie-stained SDS-PAGE gel showing purified EcPAPR4cys. (b) 4.2-K/53-mT Mössbauer spectra of 1 mM EcPAPR4cys. Experimental spectra are shown as vertical bars. The line is a quadrupole doublet simulation with the following parameters: (– –) δ_1 = 0.45 mm/s, ΔE_{Q1} = 1.03 mm/s (82%), and (···) δ_2 = 0.27 mm/s, $\Delta E_{Q,2}$ = 0.57 mm/s (15%). The parameters for the majority species (– –) are consistent with a $[4Fe\text{-}4S]^{2+}$ cluster, and the parameters for the minor species (···) are consistent with a $[2Fe\text{-}2S]^{2+}$ cluster. The remaining area of the spectrum is a broad featureless absorbing species that accounts for approximately 3% of the total area of the spectrum. (c) EPR spectrum of photoreduced EcPAPR4cys. Anaerobic EcPAPR4cys (250 μM) was photoreduced (see Methods in Supporting Information). The EPR spectrum was recorded at 10 K, and the instrument parameters were microwave power, 10 mW; receiver gain, 2 × 10^4; modulation amplitude, 10 G; and microwave frequency, 9.43 GHz.

signals from g = 2.33 to 1.58 indicate low reduction efficiency (0.04 spins mol^{-1} compared to 0.4 spins mol^{-1} for MtAPR). A possible explanation for the lower signal intensity is that the

dx.doi.org/10.1021/cb200261n | *ACS Chem. Biol.* 2012, 7, 306–315

constellation of residues surrounding the EcPAPR4cys cluster differs from APR, resulting in distinct electronic environments and reduction potentials (Supplementary Figure 2, panels c and d). In addition, we attempted to measure changes in the EPR spectrum of EcPAPR4cys that might occur on substrate binding; however, the resulting signal became too weak to be detected (data not shown). Nonetheless, the overall similarity of Mössbauer and EPR parameters to those observed for MtAPR provides further support for the coordination of a $[4Fe\text{-}4S]^{2+}$ cluster by EcPAPR4cys.

We next evaluated the effect of the [4Fe-4S] cluster in EcPAPR4cys on the ability of EcPAPR to use PAPS or APS as substrates. To this end, we first monitored formation of the *S*-sulfocysteine intermediate, which is stable in plant and bacterial (P)APRs in the absence of Trx.[6,27] EcPAPR4cys was incubated in the presence or absence of APS or PAPS, and the mass of the intact protein was analyzed by electrospray ionization mass spectrometry (ESI-MS). The deconvoluted m/z values obtained from these experiments are listed in Supplementary Table 2. In the absence of substrate, the mass spectrum of EcPAPR4cys is consistent with the molecular weight of the apoenzyme (Figure 5, panel a). Incubation of EcPAPR4cys with PAPS resulted in formation of a new series of ions with a molecular weight 80 Da higher than that of enzyme alone, corresponding to the *S*-sulfocysteine adduct (Figure 5, panel b). In the presence of APS two series of ions were observed corresponding to molecular weight of the apoenzyme (Figure 5, panel c) and to the *S*-sulfocysteine intermediate (Figure 5, panel c). Quantitative adduct formation was likely limited by our finding that not all EcPAPR4cys monomers are associated with a [4Fe-4S] cluster. Control experiments performed with wild-type enzymes and native substrates also showed the expected mass shifts (Supplementary Table 2). These data show that EcPAPR4cys can generate the adduct with PAPS or APS as a substrate.

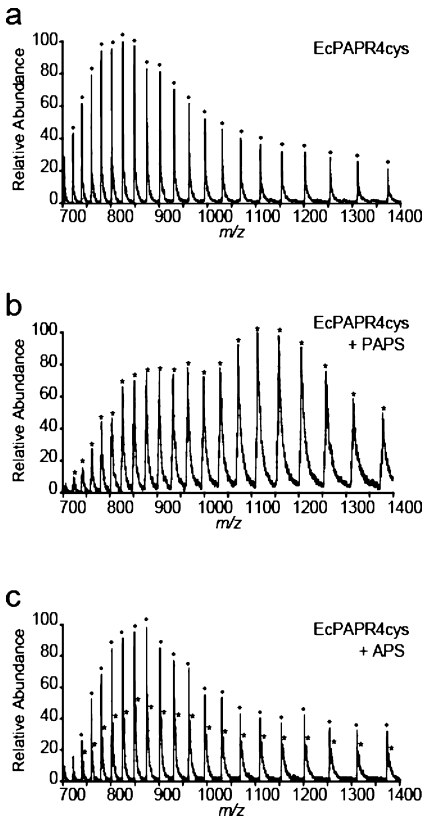

Figure 5. Mass analysis of intact EcPAPR4cys. ESI-MS of 10 μM EcPAPR4cys (a) without ligand, (b) with PAPS, and (c) with APS. Ions correspond to the enzyme (E, •) and the covalent enzyme *S*-sulfocysteine intermediate ($E\text{-}SO_3^-$, *). The calculated masses after deconvolution of m/z values are (a) 28829.23 Da, (b) 28908.55 Da, (c) 28829.23 and 28909.54 Da. MS analysis was performed under denaturing conditions, generating the apoenzyme without the iron–sulfur cluster.

As reported above, EcPAPR4cys forms an enzyme *S*-sulfocysteine intermediate with APS, which should be competent for reduction by Trx to generate sulfite. To test this possibility, we performed gel-labeling experiments with $[^{35}S]$-labeled PAPS or APS (Supplementary Figure 3). Incubation of $[^{35}S]$-PAPS or $[^{35}S]$-APS with EcPAPR4cys and analysis of the reaction by nonreducing SDS-PAGE showed a radioactive band at the molecular weight of EcPAPR indicating transfer of the $[^{35}S]$-label to the enzyme. Addition of Trx to this enzyme intermediate resulted in the complete loss of radiolabeling, as expected for reduction of the thio-sulfate bond. Analogous experiments were carried out using wild-type EcPAPR, which demonstrated comparable labeling with $[^{35}S]$-PAPS; by contrast, only a faint band was seen in reactions that contained $[^{35}S]$-APS. Taken together, the MS and radiolabeling experiments demonstrate that EcPAPR4cys forms a catalytically competent *S*-sulfocysteine intermediate with PAPS or APS and that the variant reacts with APS with an enhanced rate compared with wild-type protein.

Having established that the EcPAPR4cys iron–sulfur protein exhibits activity, we proceeded to measure kinetic parameters for this variant. Table 2 shows the resultant data and is presented alongside data obtained for wild-type EcPAPR and PaAPR (see also Supplementary Figures 4–9). The second-order rate constant also known as the specificity constant (k_{cat}/K_m; representing the reaction for free enzyme and substrate) demonstrates that EcPAPR4cys catalyzes APS reduction with approximately 600-fold less efficiency relative to PaAPR. Importantly, however, that the rate of APS reduction by the variant protein is nearly 1000-fold increased compared to wild-type EcPAPR. On the other hand, the k_{cat}/K_m for reaction of EcPAPR4cys with PAPS is almost the same as the native enzyme.

The preceding data indicate that the iron–sulfur cluster in EcPAPR4cys contributes to catalytic efficiency by enhancing substrate affinity and/or stabilizing the catalytic transition state. To gain further insight into the role of the iron–sulfur cluster in these rate enhancements, we evaluated the saturating single-turnover rate constant (k_{max}) and the $K_{1/2}$ for EcPAPR4cys and wild-type enzymes (Table 2). These data reveal that EcPAPR4cys exhibits a 100-fold increase in the value of k_{max} for APS relative to EcPAPR, while the k_{max} for PAPS was the same within error. A 9-fold enhancement in the $K_{1/2}$ of PAPS was observed for EcPAPR4cys compared to wild-type, but differences in the $K_{1/2}$ of APS could not be discerned due to the limitations imparted by the maximum achievable enzyme concentration. As expected, the $K_{1/2}$ values for all enzymes with cognate substrate were 10^2- to 10^3-fold greater relative to the non-cognate substrate. The binding of AMP and PAP to the aforementioned enzymes was also examined. The resulting K_d values indicate that incorporation of the iron–sulfur cluster in EcPAPR diminishes ligand binding by 1.5- to 3-fold (Table 2), suggesting that increased electrostatic repulsion from the negatively charged $[Fe_4S_4(Cys)_4]^{2-}$ center may hamper binding

dx.doi.org/10.1021/cb200261n|*ACS Chem. Biol.* 2012, 7, 306–315

of the 5′-phosphate dianion. Collectively, these results demonstrate that the iron−sulfur cluster in EcPAPR enhances substrate binding and APS reduction.

Finally, we evaluated the time-dependent inactivation of EcPAPR and EcPAPR4cys under prolonged exposure to aerobic conditions (Figure 6). In the case of EcPAPR4cys, dissociation of the iron−sulfur cluster from the protein scaffold could also be monitored by loss of absorption at 410 nm. Our data show that the half-life of EcPAPR, which lacks the cluster, was ∼35 h (Figure 6, panel a). However, inactivation and concomitant cluster decomposition for EcPAPR4cys occurred at an enhanced rate, with a half-life of ∼10 h (Figure 6, panels b and c). A strong correlation between an intact iron−sulfur cluster and catalytic activity is consistent with previous data obtained from plant and bacterial APRs.[11,17−19]

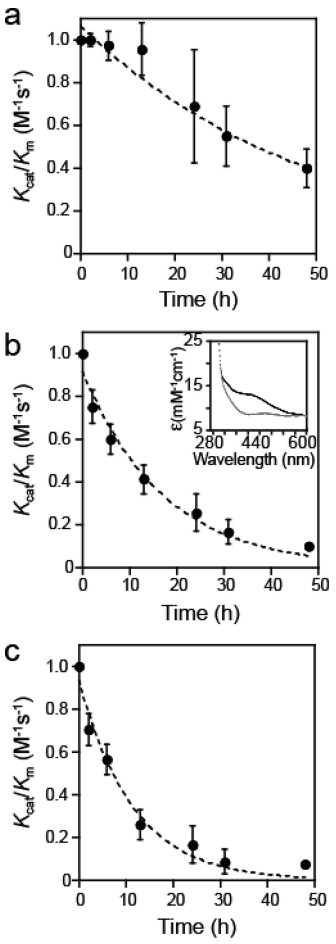

Figure 6. Time-dependent inactivation of SRs. Proteins at 10 μM were exposed to aerobic conditions at 4 °C over 2 days. At the indicated times, each enzyme was analyzed for its ability to catalyze the reduction of APS or PAPS. (a) EcPAPR with PAPS, (b) EcPAPR4cys with APS, and (c) EcPAPR4cys with PAPS. Inset in panel b shows the UV−vis absorption spectra of EcPAPR4cys at time 0 (black trace) and 48 h (gray trace).

Assimilatory sulfonucleotide reductases, APR and PAPR, exhibit similar sequences, structure, and thiol reaction chemistry.[6−9] Analysis of the phylogenetic distribution of SRs suggests that PAPR evolved from APR through a single horizontal gene transfer event.[10] The conserved reaction mechanism serves as a template for the divergent evolution of these two subclasses, which catalyze the reduction of substrates that differ by a single

Table 2. Single-Turnover Rate and Equilibrium Constants for PaAPR, EcPAPR, and EcPAPR4cys[a]

enzyme	iron content (mol Fe/mol protein)	k_{cat}/K_m[b] (M^{-1} min^{-1})		k_{max}[c] (min^{-1})		$K_{1/2}$ (μM)		K_d^{AMP} (μM)[g]	K_d^{PAP} (μM)[g]
		APS	PAPS	APS	PAPS	APS[d]	PAPS[e]		
PaAPR	3.5	2.2×10^7	1.2×10^3	3.1	$\leq 1 \times 10^{-3}$	0.1	≥100[f]	35	8.1×10^3
EcPAPR	≤0.1	≤40	3.2×10^6	$\leq 1 \times 10^{-3}$	1.6	≥100[f]	0.9	3.4×10^3	1.4
EcPAPR4cys	2.3	3.9×10^4	6.8×10^6	0.1	1.8	≥100[f]	0.1	5.6×10^3	4.3

[a]Measurements represent the average of three or more independent determinations, and the SD was ≤15% of the value in all cases. The concentration of protein was determined by quantitative amino acid analysis and corrected by the amount of active enzyme. Unless otherwise stated, reaction conditions were 100 mM Bis-Tris propane, pH 6.5, 5 mM dithiothreitol, and 10 μM thioredoxin at 30 °C. [b]k_{cat}/K_m values were measured as described in Supporting Methods. [c]k_{max} measured with saturating enzyme. [d]10 nM or [e]1 μM thioredoxin was used to measure $K_{1/2}$ values for sulfite production, by varying the concentration of enzyme. [f]At high concentrations of enzyme, the reactions became too fast to measure by hand. [g]K_d measured at pH 7.5.

3′-phosphate group. There are over 15 such enzyme families with common reaction mechanisms despite differences in substrate utilization.[15,28] In divergent evolution, protein folds and active site structural features are frequently reused among different family members and adapted to new catalytic purposes.[10] Indeed, a closer look at the active sites of PaAPR and EcPAPR reveals that several strictly conserved positively charged lysine and arginine residues interact with the sulfate moiety or α-phosphate (Figure 7 and Supplementary Figure 2). Moreover, the

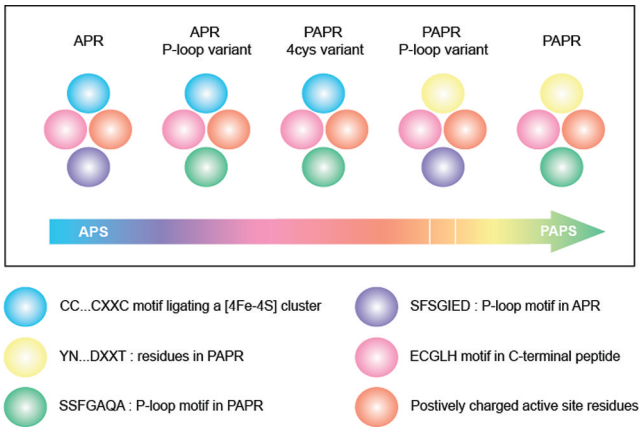

Figure 7. Model for divergent evolution of PAPR from APR. APR and PAPR can be considered to be at the margins of divergent evolution with optimum catalytic efficiency for APS (blue) and PAPS (green), as indicated by the color spectrum in the arrow. A comparison of their active sites reveals two consistent features, namely, strictly conserved positively charged lysine and arginine residues (orange circles) that interact with the substrate, and the C-terminal peptide bearing the ECGH motif, which includes the cysteine nucleophile, is also conserved (pink circles). The catalysts differ largely in their P-loop sequence motifs and their ability to ligate a [4Fe-4S] cluster through four cysteine residues. On the basis of the catalytic efficiencies for APS and PAPS, EcPAPR4cys and the P-loop variants appear to be intermediates in the evolutionary path of the functional divergence of PAPR from APR. The catalytic efficiency of the P-loop variants of EcPAPR for PAPS is lower than that of EcPAPR4cys for PAPS and is therefore indicated by a break in the arrow.

C-terminal peptide segment bearing the ECGH motif, which includes the cysteine nucleophile, is also conserved. However, two critical features distinguish APR and PAPR active sites: residues in the P-loop region and the presence/absence of an iron−sulfur cluster. These distinctions afford a unique opportunity to explore substrate recognition and identify underlying principles that govern specific features of APR that were targeted for alteration during the specialization of PAPR function.

GTP/ATP-dependent proteins contain a glycine-rich motif with the sequence GXXGXGKT/S, known as the P-loop.[7,29,30] This structural moiety forms a large anion hole that interacts with phosphates. ATP pyrophosphatases (ATP PPases) harbor a modified P-loop, also known as the PP motif,[31] with the fingerprint peptide SGGXDS/T. A highly modified version of the PP motif was discovered in EcPAPR (SXG), which is also found in enzymes with homologous protein folds, including ATP sulfurylase and GMP synthetase.[31−33] Among ATP PPases, the P-loop interacts with the 5′-phosphates of ATP.[33,34] Interestingly, however, structures of APR and PAPR co-crystallized with nucleotides show that the 3′-group on the ribose interacts with residues in the P-loop.[8,9] In SRs, the motif is characterized by the hydrophobic β1-strand and α3-helix that flank the N- and C-terminal sides of the SFS−GAED and SSSFGIQA sequences in PaAPR and EcPAPR, respectively. Differences in the P-loop motif have also been observed in ATP synthases, wherein the sequence alterations have been suggested to imply diversity in nucleotide recognition and/or catalytic mechanism.[24] Since SRs share a common catalytic mechanism, the change in P-loop sequences, particularly the acidic residues in APR, could be implicated in substrate discrimination.

In this study, site-directed mutagenesis of the P-loop entailed the replacement of negatively charged E65 and D66 PaAPR residues with corresponding neutral glutamine and alanine residues found in EcPAPR and *vice versa*. Characterization of the resulting variants has led to two significant observations. First, any change in P-loop residues had an adverse effect on catalytic efficiency, underscoring the essential nature of these highly conserved motifs in the two subclasses of catalysts. Second, variants of APR exhibited only a modest enhancement in PAP binding. This finding indicates that while neutral P-loop residues contribute somewhat to accommodating the 3′-phosphate group, they cannot account entirely for substrate specificity. Moreover, P-loop variants of PAPR did not enhance binding to AMP, showing that the mere presence of a negatively charged residue in the P-loop sequence was insufficient. Along these lines, it is possible that additional P-loop modifications are required to enhance the binding of PAPS. For instance, EcPAPR S52 and S53 (of the **SS**FGIQA sequence) establish hydrogen bonds with the 3′-phosphate group of PAPS, whereas the corresponding residues in PaAPR (of the **SF**SGAED sequence) do not make any contact with the APS 3′-hydroxyl group. Future experiments will be required to delineate this and other possibilities.

The second distinguishing feature among SRs is that APR contains the conserved cysteine sequence, CC...CXXC, which ligates an essential [4Fe-4S] cluster. Replacement of any cluster-coordinating cysteine by serine results in a complete loss of cofactor and APR activity.[17] In place of this cofactor, PAPR possesses the semiconserved motif YN...DXXT that links the α7-helix and C-terminal β-turn by hydrogen bond interactions. In the course of our study, we attempted to substitute the cysteine pairs in PaAPR with the entire YN...DXXT motif in EcPAPR (Figure 2, panels d and e); however, this quadruple variant of PaAPR failed to express in *E. coli* (data not shown). As an alternative approach to investigate the role of this region, we engineered an iron−sulfur cluster into EcPAPR. Based on the high degree of sequence and structural homology between SRs, an empirical approach was adopted to generate the new metal-binding site. This strategy has been employed to design novel metalloproteins, including the creation of a Mn(II)-binding site in cytochrome *c* peroxidase based on structural homology with manganese peroxidase.[35,36] Favorable protein folds such as the Trx scaffold have also been exploited to introduce a cofactor and alter enzyme function.[37] Assembly of a [2Fe-2S] cluster through directed evolution served to bridge two monomeric Trx subunits and enabled the resulting dimer to catalyze oxygen-dependent sulfhydryl oxidation.[38,39] In another instance, the second cysteine residue of the native CXXXCXXXC motif in the catalytic subunit of dimethyl-sulfoxide reductase (DmsA) was replaced leading to the assembly of a paramagnetic [3Fe-4S] cluster.[40]

In the case of EcPAPR, our goal was to introduce a [4Fe-4S] cluster in order to probe the role of the metallocenter in

sulfonucleotide reduction. A combination of UV/vis, EPR, and Mössbauer spectroscopies, mass spectroscopy, and kinetic analyses were employed to characterize the resulting variant, EcPAPR4cys. Though we did not identify conditions that permitted quantitative cluster incorporation into each protein monomer, our spectroscopic data provides strong support for the assignment of a $[Fe_4S_4(Cys)_4]^{2-}$ center and compares favorably with studies of MtAPR.[16] Comparison of k_{cat}/K_m between EcPAPR4cys with wild-type PaAPR and EcPAPR showed that the installation of an iron−sulfur cluster dramatically improved the ability to turn over the APS ($\sim 10^3$-fold). Further studies revealed a minor role in substrate binding, with the majority of the rate enhancement stemming from the improvement in k_{max}, which reports on the rate of the chemical step. Furthermore, time-dependent inactivation studies also showed that the cluster was required for catalytic activity.

Previously, using EPR spectroscopy, we have observed electrostatic interactions between the iron−sulfur cluster, a conserved active site lysine residue, and the ligand bound to APR.[16] The intimate connection between these active site elements was further established through computational analysis.[41] On the basis of these studies and the crystal structure of the ligand-protein complex (Supplementary Figure 2), we have proposed that the $[Fe_4S_4(Cys)_4]^{2-}$ cluster cofactor plays a role preorganizing positively charged active site residues and in substrate activation. Along these lines, it is possible that the engineered iron-cluster in PAPR4cys may facilitate contact between the conserved lysine and APS. The resulting network of electrostatic interactions could be exploited to promote catalysis. Specifically, the charge from and polarization within the iron−sulfur cluster could serve to activate the 5′-sulfate group, thereby facilitating S−OP cleavage and S−S bond formation during the reaction. In the absence of an iron−sulfur cluster, PAPR could achieve something similar *via* repulsion between the extra 3′-phosphate group of PAPS and the sulfate end of the 5′-phosphosulfate. Our observation, that insertion of an iron−sulfur cluster in PAPR enhances the rate of APS reduction, is entirely consistent with this model. In this regard, iron−sulfur clusters are extremely versatile cofactors with enzymatic functions in electron transfer, Lewis acid assisted catalysis, radical generation, and source of sulfur during biosyntheses of cofactors.[42−49] This present study extends this list of functions to include substrate specificity.

From our study and sequence analysis, it is clear that the natural evolution of PAPR from APR involved several iterations of mutations. These factors are not easily recapitulated, and we note that none of the variants explored in this study resulted in a complete change of substrate specificity.[50] Functional studies of EcPAPR4cys and the P-loop variants suggest that these enzymes may represent intermediates in the evolutionary pathway of SRs (Figure 7). This proposal is based on two interesting observations related to the catalytic efficiency and relative stability. First is the striking similarity between (P)APR from *B. subtilis* and the P-loop variants of PaAPR. These enzymes coordinate an iron−sulfur cluster but also contain a neutral residue in the position equivalent to residue 66 of PaAPR (or position 58 of EcPAPR). However, these catalysts all exhibit a significant reduction in catalytic efficiency with APS ($\geq 10^2$) compared to wild-type PaAPR (Table 1). Second, like APR-B from *P. patens*, the EcPAPR P-loop variants lack the iron−sulfur cluster and also display a decrease in enzyme activity relative to wild-type PaAPR (Table 1). Interestingly, we note that both PpAPR-B and EcPAPR gain in stability by forfeiting the iron−sulfur cluster. EcPAPR retains enzymatic activity over 2 days in contrast to APR, which loses activity within half a day. Similarly, PpAPR-B remains active for 5 days compared to its homologue, PpAPR, which harbors a [4Fe-4S] cluster and is only active for 2 days under aerobic conditions.[19] Finally, we note that both BsAPR and PpAPR-B have markedly decreased catalytic efficiency relative to that of other SRs (Table 1), indicating that these enzymes are not as specialized for the reductase function as the latter group of catalysts. Taken together, these observations show how characteristics of our experimentally generated variants resemble those of SRs from naturally occurring species, corroborating our proposal that the variants are representative of intermediates in the path of divergent evolution of PAPR from APR (Figure 7).

In conclusion, the cysteine motif that coordinates the [4Fe-4S] cluster within APR can be accommodated by the PAPR scaffold and confers enhanced binding and catalytic activity for the APS substrate. This work provides valuable insight into the contribution of the iron−sulfur cluster to catalysis and a better understanding of the mechanisms involved in the divergent evolution of PAPR from APR.

METHODS

APS (≥95%) was obtained from Biolog Life Sciences Institute (Bremen, Germany). PAPS (≥88%) was obtained from Calbiochem. PAP, AMP, iron(III) chloride were purchased from Sigma-Aldrich. Fe-57 metal was purchased from Isoflex USA and micro biospin P30 columns were from Bio-Rad Laboratories. Protein concentrations were determined by quantitative amino acid analysis (Molecular Structure Facility, UC-Davis, CA) and corrected by the number of active molecules,[6] as detailed in Supporting Information. The Fe content of each protein preparation was determined in duplicate by inductively coupled plasma (ICP) analysis. Full details for SR purification, spectroscopic, and kinetic Methods are reported in the Supporting Information.

ASSOCIATED CONTENT

Supporting Information

This material is available free of charge *via* the Internet at http://pubs.acs.org.

AUTHOR INFORMATION

Corresponding Author

*E-mail: kcarroll@scripps.edu.

ACKNOWLEDGMENTS

We thank the National Institutes of Health for financial support (GM087638 to K.S.C.).

REFERENCES

(1) Schwenn, J. D. (1994) Photosynthetic sulfate reduction. *Z. Naturforsch. 49c*, 531−539.

(2) Kredich, N. M. (1996) *Escherichia coli and Salmonella typhimurium: Cellular and Molecular Biology*, Vol. *1*, 2nd ed., ASM Press, Washington, DC.

(3) Schelle, M. W., and Bertozzi, C. R. (2006) Sulfate metabolism in mycobacteria. *ChemBioChem 7*, 1516−1524.

(4) Williams, S. J., Senaratne, R. H., Mougous, J. D., Riley, L. W., and Bertozzi, C. R. (2002) 5′-Adenosinephosphosulfate lies at a metabolic branch point in mycobacteria. *J. Biol. Chem. 277*, 32606−32615.

(5) Senaratne, R. H., De Silva, A. D., Williams, S. J., Mougous, J. D., Reader, J. R., Zhang, T., Chan, S., Sidders, B., Lee, D. H., Chan, J., Bertozzi, C. R., and Riley, L. W. (2006) 5′-Adenosinephosphosulphate reductase (CysH) protects *Mycobacterium tuberculosis* against free

radicals during chronic infection phase in mice. *Mol. Microbiol. 59*, 1744−1753.
(6) Carroll, K. S., Gao, H., Chen, H., Stout, C. D., Leary, J. A., and Bertozzi, C. R. (2005) A conserved mechanism for sulfonucleotide reduction. *PLoS Biol. 3*, e250.
(7) Savage, H., Montoya, G., Svensson, C., Schwenn, J. D., and Sinning, I. (1997) Crystal structure of phosphoadenylyl sulphate (PAPS) reductase: a new family of adenine nucleotide alpha hydrolases. *Structure 5*, 895−906.
(8) Chartron, J., Carroll, K. S., Shiau, C., Gao, H., Leary, J. A., Bertozzi, C. R., and Stout, C. D. (2006) Substrate recognition, protein dynamics, and iron-sulfur cluster in *Pseudomonas aeruginosa* adenosine 5′-phosphosulfate reductase. *J. Mol. Biol. 364*, 152−169.
(9) Yu, Z., Lemongello, D., Segel, I. H., and Fisher, A. J. (2008) Crystal structure of *Saccharomyces cerevisiae* 3′-phosphoadenosine-5′-phosphosulfate reductase complexed with adenosine 3′,5′-bisphosphate. *Biochemistry 47*, 12777−12786.
(10) Kopriva, S., Buchert, T., Fritz, G., Suter, M., Benda, R., Schünemann, V., Koprivova, A., Schürmann, P., Trautwein, A. X., Kroneck, P. M., and Brunold, C. (2002) The presence of an iron-sulfur cluster in adenosine 5′-phosphosulfate reductase separates organisms utilizing adenosine 5′-phosphosulfate and phosphoadenosine 5′-phosphosulfate for sulfate assimilation. *J. Biol. Chem. 277*, 21786−21791.
(11) Kopriva, S., Buchert, T., Fritz, G., Suter, M., Weber, M., Benda, R., Schaller, J., Feller, U., Schürmann, P., Schünemann, V., Trautwein, A. X., Kroneck, P. M., and Brunold, C. (2001) Plant adenosine 5′-phosphosulfate reductase is a novel iron-sulfur protein. *J. Biol. Chem. 276*, 42881−42886.
(12) Setya, A., Murillo, M., and Leustek, T. (1996) Sulfate reduction in higher plants: molecular evidence for a novel 5′-adenylylsulfate reductase. *Proc. Natl. Acad. Sci. U.S.A. 93*, 13383−13388.
(13) Kim, S. K., Rahman, A., Conover, R. C., Johnson, M. K., Mason, J. T., Gomes, V., Hirasawa, M., Moore, M. L., Leustek, T., and Knaff, D. B. (2006) Properties of the cysteine residues and the iron-sulfur cluster of the assimilatory 5′-adenylyl sulfate reductase from *Enteromorpha intestinalis*. *Biochemistry 45*, 5010−5018.
(14) Kim, S. K., Gomes, V., Gao, Y., Chandramouli, K., Johnson, M. K., Knaff, D. B., and Leustek, T. (2007) The two-domain structure of 5′-adenylylsulfate (APS) reductase from *Enteromorpha intestinalis* is a requirement for efficient APS reductase activity. *Biochemistry 46*, 591−601.
(15) Chartron, J., Shiau, C., Stout, C. D., and Carroll, K. S. (2007) 3′-Phosphoadenosine-5′-phosphosulfate reductase in complex with thioredoxin: a structural snapshot in the catalytic cycle. *Biochemistry 46*, 3942−3951.
(16) Bhave, D. P., Hong, J. A., Lee, M., Jiang, W., Krebs, C., and Carroll, K. S. (2011) Spectroscopic studies on the [4Fe-4S] cluster in adenosine 5′-phosphosulfate reductase from *Mycobacterium tuberculosis*. *J. Biol. Chem. 286*, 1216−1226.
(17) Carroll, K. S., Gao, H., Chen, H., Leary, J. A., and Bertozzi, C. R. (2005) Investigation of the iron-sulfur cluster in *Mycobacterium tuberculosis* APS reductase: implications for substrate binding and catalysis. *Biochemistry 44*, 14647−14657.
(18) Berndt, C., Lillig, C. H., Wollenberg, M., Bill, E., Mansilla, M. C., de Mendoza, D., Seidler, A., and Schwenn, J. D. (2004) Characterization and reconstitution of a 4Fe-4S adenylyl sulfate/phosphoadenylyl sulfate reductase from *Bacillus subtilis*. *J. Biol. Chem. 279*, 7850−7855.
(19) Kopriva, S., Fritzemeier, K., Wiedemann, G., and Reski, R. (2007) The putative moss 3′-phosphoadenosine-5′-phosphosulfate reductase is a novel form of adenosine-5′-phosphosulfate reductase without an iron-sulfur cluster. *J. Biol. Chem. 282*, 22930−22938.
(20) Penning, T. M., and Jez, J. M. (2001) Enzyme redesign. *Chem. Rev. 101*, 3027−3046.
(21) Scrutton, N. S., Berry, A., and Perham, R. N. (1990) Redesign of the coenzyme specificity of a dehydrogenase by protein engineering. *Nature 343*, 38−43.
(22) Shah, K., Liu, Y., Deirmengian, C., and Shokat, K. M. (1997) Engineering unnatural nucleotide specificity for Rous sarcoma virus tyrosine kinase to uniquely label its direct substrates. *Proc. Natl. Acad. Sci. U.S.A. 94*, 3565−3570.
(23) Bishop, A. C., Ubersax, J. A., Petsch, D. T., Matheos, D. P., Gray, N. S., Blethrow, J., Shimizu, E., Tsien, J. Z., Schultz, P. G., Rose, M. D., Wood, J. L., Morgan, D. O., and Shokat, K. M. (2000) A chemical switch for inhibitor-sensitive alleles of any protein kinase. *Nature 407*, 395−401.
(24) Bhave, D. P., Muse, W. B. 3rd, and Carroll, K. S. (2007) Drug targets in mycobacterial sulfur metabolism. *Infect. Disord.: Drug Targets 7*, 140−158.
(25) Mdluli, K., and Spigelman, M. (2006) Novel targets for tuberculosis drug discovery. *Curr. Opin. Pharmacol. 6*, 459−467.
(26) Johnson, D. C., Unciuleac, M. C., and Dean, D. R. (2006) Controlled expression and functional analysis of iron-sulfur cluster biosynthetic components within *Azotobacter vinelandii*. *J. Bacteriol. 188*, 7551−7561.
(27) Weber, M., Suter, M., Brunold, C., and Kopriva, S. (2000) Sulfate assimilation in higher plants characterization of a stable intermediate in the adenosine 5′-phosphosulfate reductase reaction. *Eur. J. Biochem. 267*, 3647−3653.
(28) Suter, M., von Ballmoos, P., Kopriva, S., den Camp, R. O., Schaller, J., Kuhlemeier, C., Schürmann, P., and Brunold, C. (2000) Adenosine 5′-phosphosulfate sulfotransferase and adenosine 5′-phosphosulfate reductase are identical enzymes. *J. Biol. Chem. 275*, 930−936.
(29) Dreusicke, D., and Schulz, G. E. (1986) The glycine-rich loop of adenylate kinase forms a giant anion hole. *FEBS Lett. 208*, 301−304.
(30) Saraste, M., Sibbald, P. R., and Wittinghofer, A. (1990) The P-loop-a common motif in ATP- and GTP-binding proteins. *Trends Biochem. Sci. 15*, 430−434.
(31) Bork, P., and Koonin, E. V. (1994) A P-loop-like motif in a widespread ATP pyrophosphatase domain: implications for the evolution of sequence motifs and enzyme activity. *Proteins 20*, 347−355.
(32) Mougous, J. D., Lee, D. H., Hubbard, S. C., Schelle, M. W., Vocadlo, D. J., Berger, J. M., and Bertozzi, C. R. (2006) Molecular basis for G protein control of the prokaryotic ATP sulfurylase. *Mol. Cell 21*, 109−122.
(33) Tesmer, J. J., Klem, T. J., Deras, M. L., Davisson, V. J., and Smith, J. L. (1996) The crystal structure of GMP synthetase reveals a novel catalytic triad and is a structural paradigm for two enzyme families. *Nat. Struct. Biol. 3*, 74−86.
(34) Smith, C. A., and Rayment, I. (1996) Active site comparisons highlight structural similarities between myosin and other P-loop proteins. *Biophys. J. 70*, 1590−1602.
(35) Yeung, B. K., Wang, X., Sigman, J. A., Petillo, P. A., and Lu, Y. (1997) Construction and characterization of a manganese-binding site in cytochrome c peroxidase: towards a novel manganese peroxidase. *Chem. Biol. 4*, 215−221.
(36) Wilcox, S. K., Putnam, C. D., Sastry, M., Blankenship, J., Chazin, W. J., McRee, D. E., and Goodin, D. B. (1998) Rational design of a functional metalloenzyme: introduction of a site for manganese binding and oxidation into a heme peroxidase. *Biochemistry 37*, 16853−16862.
(37) Coldren, C. D., Hellinga, H. W., and Caradonna, J. P. (1997) The rational design and construction of a cuboidal iron-sulfur protein. *Proc. Natl. Acad. Sci. U.S.A. 94*, 6635−6640.
(38) Masip, L., Pan, J. L., Haldar, S., Penner-Hahn, J. E., DeLisa, M. P., Georgiou, G., Bardwell, J. C., and Collet, J. F. (2004) An engineered pathway for the formation of protein disulfide bonds. *Science 303*, 1185−1189.
(39) Collet, J. F., Peisach, D., Bardwell, J. C., and Xu, Z. (2005) The crystal structure of TrxA(CACA): Insights into the formation of a [2Fe-2S] iron-sulfur cluster in an *Escherichia coli* thioredoxin mutant. *Protein Sci. 14*, 1863−1869.
(40) Trieber, C. A., Rothery, R. A., and Weiner, J. H. (1996) Engineering a novel iron-sulfur cluster into the catalytic subunit of *Escherichia coli* dimethyl-sulfoxide reductase. *J. Biol. Chem. 271*, 4620−4626.

(41) Bhave, D. P., Han, W. G., Pazicni, S., Penner-Hahn, J. E., Carroll, K. S., and Noodleman, L. (2011) Geometric and electrostatic study of the [4Fe-4S] cluster of adenosine-5′-phosphosulfate reductase from broken symmetry density functional calculations and extended X-ray absorption fine structure spectroscopy. *Inorg. Chem. 50*, 6610−6625.
(42) Booker, S. J. (2009) Anaerobic functionalization of unactivated C-H bonds. *Curr. Opin. Chem. Biol. 13*, 58−73.
(43) Dos Santos, P. C., and Dean, D. R. (2008) A newly discovered role for iron-sulfur clusters. *Proc. Natl. Acad. Sci. U.S.A. 105*, 11589−11590.
(44) Beinert, H., Holm, R. H., and Münck, E. (1997) Iron-sulfur clusters: nature's modular, multipurpose structures. *Science 277*, 653−659.
(45) Beinert, H., Kennedy, M. C., and Stout, C. D. (1996) Aconitase as Iron-sulfur protein, enzyme, and iron-regulatory protein. *Chem. Rev. 96*, 2335−374.
(46) Walsby, C. J., Ortillo, D., Yang, J., Nnyepi, M. R., Broderick, W. E., Hoffman, B. M., and Broderick, J. B. (2005) Spectroscopic approaches to elucidating novel iron-sulfur chemistry in the "radical-SAM" protein superfamily. *Inorg. Chem. 44*, 727−741.
(47) Fontecave, M. (2006) Iron-sulfur clusters: ever-expanding roles. *Nat. Chem. Biol. 2*, 171−174.
(48) Frey, P. A., Hegeman, A. D., and Ruzicka, F. J. (2008) The radical SAM superfamily. *Crit. Rev. Biochem. Mol. Biol. 43*, 63−88.
(49) Booker, S. J., Cicchillo, R. M., and Grove, T. L. (2007) Self-sacrifice in radical *S*-adenosylmethionine proteins. *Curr. Opin. Chem. Biol. 11*, 543−552.
(50) Hong, J. A., Bhave, D. P., and Carroll, K. S. (2009) Identification of critical ligand binding determinants in *Mycobacterium tuberculosis* adenosine-5′-phosphosulfate reductase. *J. Med. Chem. 52*, 5485−5495.